

Structures of the Bacterial Ribosome in Classical and Hybrid States of tRNA Binding

Jack A. Dunkle,^{1*} Leyi Wang,² Michael B. Feldman,^{2,3} Arto Pulk,¹ Vincent B. Chen,⁴ Gary J. Kapral,⁴ Jonas Noeske,¹ Jane S. Richardson,⁴ Scott C. Blanchard,² Jamie H. Doudna Cate^{1,5†}

During protein synthesis, the ribosome controls the movement of tRNA and mRNA by means of large-scale structural rearrangements. We describe structures of the intact bacterial ribosome from *Escherichia coli* that reveal how the ribosome binds tRNA in two functionally distinct states, determined to a resolution of ~3.2 angstroms by means of x-ray crystallography. One state positions tRNA in the peptidyl-tRNA binding site. The second, a fully rotated state, is stabilized by ribosome recycling factor and binds tRNA in a highly bent conformation in a hybrid peptidyl/exit site. The structures help to explain how the ratchet-like motion of the two ribosomal subunits contributes to the mechanisms of translocation, termination, and ribosome recycling.

Protein biosynthesis by the ribosome proceeds in defined phases of initiation, protein elongation, termination, and ribosome recycling (1). Understanding the molecular mechanism of translation requires high-resolution descriptions of the motions in the ribosome that enable key translational events (1–3). A ratchet-like rotation of the small ribosomal subunit relative to the large ribosomal subunit (4) is crucial to the positioning of tRNAs in intermediate—or hybrid—binding sites, in which the 3'-CCA termini and acceptor stems of tRNA advance by one site on the large subunit while the anticodon elements of tRNA remain fixed on the small subunit (5). Binding of tRNAs in hybrid sites is central to mRNA and tRNA movements on the

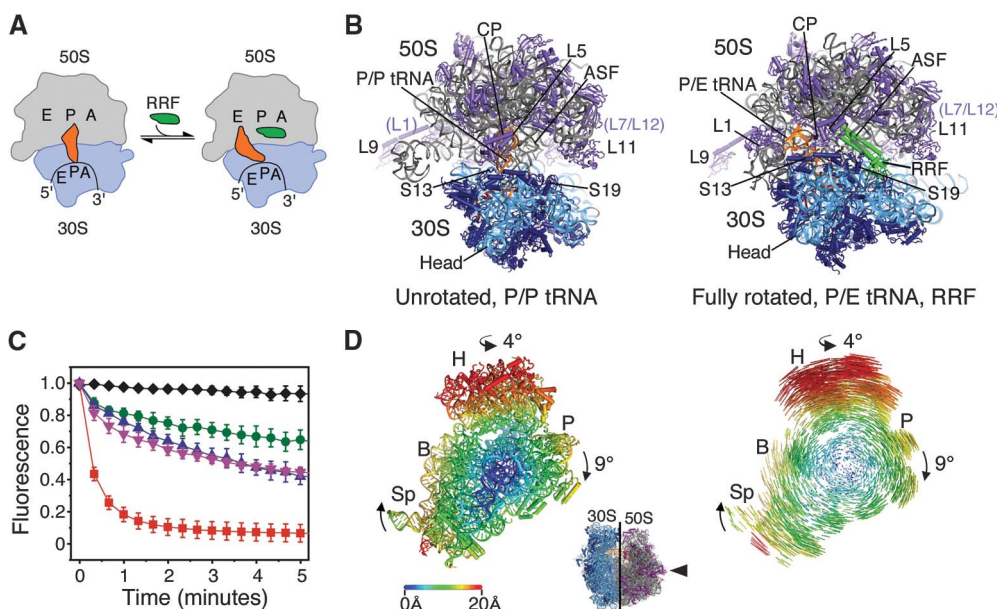
ribosome when they are translocated after each peptide bond is formed, during termination, and during ribosome recycling (6, 7). However, the molecular basis for ribosome positioning of tRNAs in hybrid sites has been unclear.

Atomic-resolution x-ray crystal structures of the bacterial ribosome with ligands bound have revealed molecular details of conformational rearrangements taking place in the unrotated ribosome (1). The first molecular descriptions of intermediate states of ribosome ratchet-like rotation at atomic resolution were provided by x-ray crystal structures of the *Escherichia coli* 70S ribosome (8), with additional substeps proposed on the basis of cryogenic electron microscopy (cryo-EM) reconstructions (9). A posttranslo-

cation rotated state of the ribosome was recently identified by means of cryo-EM (10), in a conformation similar to that of the *Saccharomyces cerevisiae* 80S ribosome in the absence of bound substrates (11, 12).

After the termination of protein synthesis, ribosome recycling is required to free ribosomes from the mRNA transcript to enable further rounds of translation. In bacteria and organelles, ribosome recycling factor (RRF) binds in the tRNA-binding cleft of the 70S ribosome at the interface of the large (50S) and small (30S) subunits and interacts with the 50S subunit peptidyl transferase center (PTC) (13, 14). In so doing, RRF sterically occludes deacylated tRNA binding in the peptidyl-tRNA site (P site, P/P configuration) to favor tRNA positioning in the hybrid peptidyl/exit tRNA-binding site (P/E configuration) (Fig. 1A) (13, 15, 16). In the P/E configuration, tRNA is bound simultaneously to the P site of the small (30S) subunit and to the E site of the large (50S) subunit (5). Binding of the guanosine triphosphatase (GTPase) elongation

Fig. 1. Ribosome recycling in bacteria and organelles. **(A)** Steps of ribosome recycling. After termination, ribosomes with deacylated tRNA in the P site undergo a structural rearrangement to a fully rotated state in which tRNA adopts a P/E hybrid state of binding and RRF is bound in the 50S P site. EF-G then catalyzes subunit dissociation. **(B)** Global views of the ribosome in a posttermination state (L) and intermediate state of recycling (R). The small subunit rRNA and proteins are colored light and dark blue, respectively, with the large subunit rRNA and proteins colored gray and purple, respectively. Bound tRNA (orange), mRNA (dark red), and RRF (green) are also shown. **(C)** The dependence of subunit release on RRF, EF-G, and GTP under crystallographic buffer conditions. Release was monitored by the loss of Cy5-labeled L1 fluorescence in 50S subunits from surface-immobilized ribosome complexes carrying Cy3-labeled tRNA^{Phe} in the P site. Complexes were imaged in the absence of factors (black diamonds) or in the presence of 10 μ M RRF (green circles), 20 μ M EF-G/2 mM GTP (purple inverted triangles), 10 μ M RRF/20 μ M EF-G/2 mM GDPNP (blue triangles), or 10 μ M RRF/20 μ M EF-G/2 mM GTP (red squares). Data reflect the mean \pm SD of normalized Cy5 fluorescence intensity as a function of time from three experimental replicates. **(D)** Conformational changes in the 70S ribosome during inter-subunit rotation. (Inset) View of the 30S subunit from the



perspective of the 50S subunit. Shifts between equivalent RNA phosphorus atoms and protein C α atoms in the unrotated (R₀) and fully rotated (R_F) states are color coded as indicated by the scale. Ribosomes were superimposed by using the 50S subunit as the frame of reference (38). Difference vectors between equivalent phosphorus or C α atoms of the 30S subunits in the unrotated and fully rotated ribosome structures are shown on the right.

factor-G (EF-G) to the RRF-ribosome complex and subsequent guanosine 5'-triphosphate (GTP) hydrolysis lead to the dissociation of ribosomal subunits (17).

We determined structures of the intact *E. coli* 70S ribosome at a resolution of ~ 3.2 Å (tables S1 and S2) (12) using crystals that contain two independent copies of the ribosome per asymmetric unit in a "top-top" polysome configuration (18). One ribosome adopts an unrotated state, with tRNA^{Phe} bound in the peptidyl-tRNA (P/P) binding site (Fig. 1B) (19) that mimics a posttermination state of the translation cycle. The second ribosome adopts a fully rotated conformation that contains tRNA^{Phe} bound in the hybrid P/E binding site and RRF bound at the ribosomal subunit interface (Fig. 1B). This structure is thought to represent an early intermediate in bacterial ribosome recycling (Fig. 1A) (15). Under these buffer conditions, single-molecule fluorescence resonance energy transfer (smFRET) measurements showed RRF achieved approximately 50% maximal stabilization of the fully rotated, P/E hybrid configuration of the posttermination complex (fig. S1) and supported EF-G- and GTP hydrolysis-dependent ribosome recycling (Fig. 1C and fig. S1) (12).

When compared with the posttermination ribosome complex, the 30S subunit of the RRF-bound ribosome is rotated $\sim 9^\circ$ relative to the 50S subunit. An approximately orthogonal rotation of the head domain of the 30S subunit of $\sim 4^\circ$ swivels the head domain in the direction of the ribosomal E site on the 50S subunit. These motions of the 30S subunit into the rotated state result in shifts at the periphery of the ribosome of more than 20 Å (Fig. 1D) that direct deacylated P-site tRNA into the P/E hybrid site. The tRNA anticodon stem-loop (ASL) and mRNA move laterally by ~ 6 Å relative to the 50S subunit, coupled to the motion of the 30S subunit platform domain (Figs. 1D and 2A). When tRNA moves into the P/E site from the P/P site, the tRNA ASL remains in contact with the 30S subunit head and platform domains (Fig. 2B and fig. S2A) (19) but breaks its interactions with 23S ribosomal RNA (rRNA) helix H69 in the large subunit (19) (Fig. 2B and movie S1).

Bound in the hybrid P/E site, tRNA^{Phe} is severely kinked at the junction between the ASL and D stem when compared with tRNA^{Phe} bound in the P/P site. Although the conformation of the anticodon and two closing base pairs of the ASL region remain essentially unchanged, the major groove widens by ~ 4 Å at the junction of the ASL and D stem (Fig. 2C and fig. S2). The kink between the ASL and D stems allows the acceptor stem of P/E tRNA to swing by $\sim 37^\circ$ into the 50S E site (Fig. 2D) (12). This abrupt kink contrasts with the more distributed bend that occurs in mRNA-decoding complexes bound to elongation factor EF-Tu [A/T state, (20, 21)], in which tRNA bends in the opposite direction. Comparing P/E tRNA with A/T tRNA, the total extent of tRNA bending at the ASL/D-stem junction amounts to $\sim 70^\circ$ (Fig. 2D and movie S1).

In the large subunit E site, P/E tRNA contacts the ribosome in a similar manner to tRNA bound in the E/E site (Fig. 2B) (19). Nucleotides G2112 and G2168 in 23S rRNA, part of the protein L1-containing arm of the 50S subunit, stack on the D-loop and T-loop of P/E tRNA (Figs. 1B and 2B) (22). Consistent with biochemical studies of the mechanism of translocation (23), nucleotide A76 at the acceptor end of P/E tRNA stacks between nucleotides in helix H88 of 23S rRNA (Fig. 2B and fig. S3), where the terminal ribose engages the Watson-Crick face of nucleotide C2394 (19, 23). In contrast to the positioning of C75 in E-site tRNA in the bacterium *Thermus thermophilus* (19) and in the archaeal large subunit (24), in the *E. coli* ribosome, nucleotide C75 in P/E tRNA stacks on nucleotide A2432 in 23S rRNA, away from the tRNA acceptor stem (fig. S3). The striking divergence of the 50S E site contacts contrasts with the high level of conservation in the peptidyl transferase center, supporting the notion that the ribosomal E site evolved relatively late and has continued to diverge (19, 25).

The molecular contacts between the two ribosomal subunits are composed of both rRNA and ribosomal proteins, with the central contacts, or bridges, conserved across kingdoms (11, 26). In the fully rotated state, the pivot point for intersubunit ratcheting occurs at bridge B3 (Fig. 3A and fig. S4), which maintains the same conformation and contacts when compared with the unrotated ribosome (26). Bridge B3 is composed

of a cross-strand adenosine-stacking motif (27), in which residues A1418 and A1483 within helix 44 (h44) of 16S rRNA in the 30S subunit dock into the minor groove of helix 71 (H71) in 23S rRNA of the 50S subunit. Residues A1418 and A1483 lie within adjacent sheared G-A base pairs that coordinate an inner-sphere magnesium ion that possibly contributes to subunit association in all organisms (Fig. 3B) (26, 28).

In the aminoacyl-tRNA (A) and P sites, bridge B2a involves contacts between 23S rRNA helix H69 in the 50S subunit and 16S rRNA residues at the end of helix h44 in the 30S subunit that are preserved in both the unrotated and fully rotated states of the ribosome (Fig. 3A). In both states, residue A1913 of H69 penetrates the minor groove of the h44 mRNA decoding site. However, in going from the unrotated to fully rotated state, the P-site tRNA anticodon, mRNA (Fig. 2A), and the end of helix h44 move laterally by ~ 6 Å toward the E site (Fig. 3C). The interactions between H69 and h44 are maintained during this movement because of a ~ 5 Å compression of H69 (Fig. 3C and movie S2). In part, this compression is enabled by disruption of the terminal base pair (C1925-G1929) of H69 and extrusion of the nearly universally conserved uridine U1926 (29) from the tight U-turn motif at the base of H69 (fig. S5 and movie S2) (25).

The observed conformational rearrangements in bridge B2a may help explain how antibiotics such as viomycin that target translocation stabi-

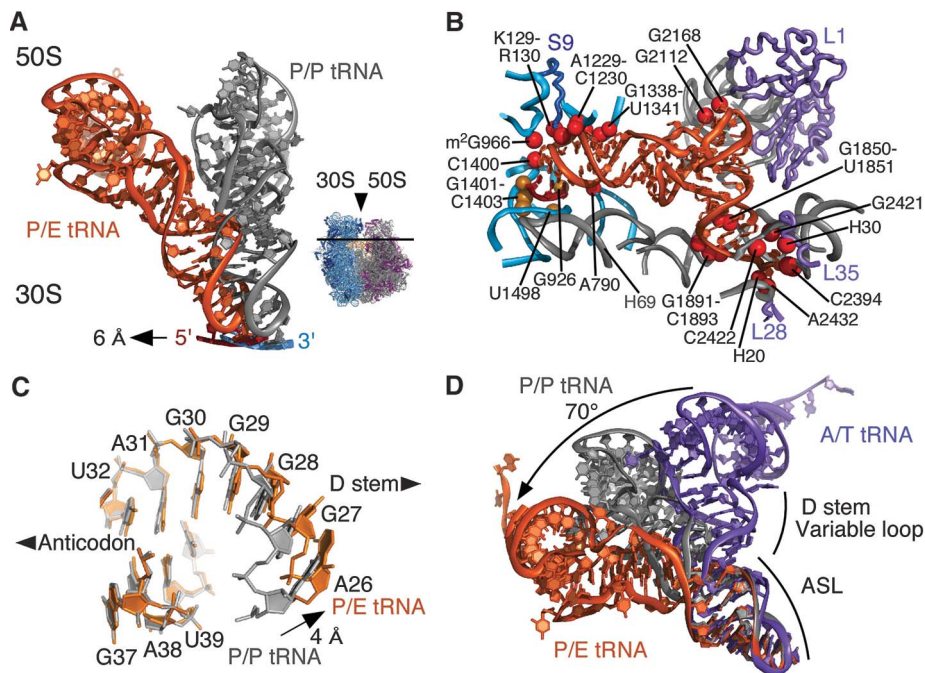


Fig. 2. Conformation of tRNA in the P/E hybrid state. (A) Movement of P/E tRNA and mRNA toward the E site when compared with P/P tRNA and mRNA. The direction of view is shown to the right. (B) View of mRNA and P/E tRNA interactions with the 30S subunit P site and 50S subunit E site. Residues that contact mRNA (gold) and P/E tRNA (red) are shown. Colors for the ribosome, mRNA, and tRNA are as in Fig. 1. (C) View of the P/E tRNA ASL/D stem junction (orange). P/P tRNA (gray) is shown for comparison, with an arrow indicating the widening of the helix major groove. (D) Comparison of ASL/D stem junctions between P/E tRNA (orange), P/P tRNA (gray), and A/T tRNA (purple). A/T tRNA structure is a homology model adapted from (12, 21). The bending angle for the A/T to P/E conformational change (70°) is shown.

lize the fully rotated state of the ribosome (30, 31). Viomycin and the related antibiotic capreomycin bind to the ribosome in the vicinity of nucleotide A1913 in 23S rRNA (32), the only nucleotide whose contacts with h44 change appreciably during inter-subunit rotation. Aminoglycosides such as neomycin, which bind to two sites in bridge B2a (33, 34), may favor the fully rotated state of the ribosome by stabilizing the compressed conformation of helix H69.

On the opposite end of the tRNA-binding cleft, bridge B7a is disrupted by the rotation of the 30S platform domain (Fig. 1D). In the unrotated state, nucleotide A702 in 16S rRNA stacks on an A-A dinucleotide platform near the end of helix H68 of 23S rRNA (12, 35). This interaction involves a hydrogen bond between N1 of A702 and G1846 in 23S rRNA (25). Consistent with chemical probing data used to identify hybrid tRNA-binding sites (5), rotation of the 30S platform domain into the

fully rotated position results in a ~ 13 Å displacement of A702 away from H68 that exposes the base pairing face of A702 to solvent (Fig. 3D). Consistent with biochemical observations (36), H68 moves in the opposite direction by 2 to 3 Å to pack in the minor groove of the acceptor stem of P/E tRNA (Fig. 3D), probably helping to stabilize tRNA in the P/E hybrid site.

The absence of bridge B7a in the fully rotated state appears to be partially compensated for by new contacts between protein L2 in the large subunit and helices h23 and h24 in 16S rRNA (bridges B7b and B7c) (Fig. 3A). However, the key stabilizing contact to the 30S platform region in both the unrotated and fully rotated ribosome configurations remains bridge B4, which in bacteria involves intimate contacts between the hairpin loop at the end of helix H34 in 23S rRNA of the large subunit and protein S15 in the small subunit. Helix H34 bends by ~ 7 Å, or 12° , during inter-subunit rotation and slightly adjusts how nucleotide A715 packs on the hydrophobic surface of protein S15 (Fig. 3E) (25). Compensation for the loss of bridge B7a in the fully rotated state may also result from the formation of more extensive interactions between the 30S subunit body domain and the 50S subunit near bridge B8. In bridge B8, large subunit proteins L14 and L19 interact more closely with helices h8 and h14 in the 30S subunit (Fig. 3A).

In the fully rotated state, the head domain of the 30S subunit swivels as a rigid body in the direction of tRNA movement, rearranging bridge B1b to place the central alpha helix of protein S13 directly across from protein L5 in the 50S subunit (Fig. 1B) (37). This lateral change in protein S13 position correlates with tRNA binding in the hybrid P/E site and may help control the position of tRNAs on the ribosome (38). Thus, the contacts between protein S13 and protein L5 probably play an important role in the ribosome ratcheting mechanism. Consistent with this view, deletions in protein S13 result in more rapid and lower fidelity translocation of mRNA and tRNA (39). Mutations in the other major contact between the 30S subunit head domain and helix H38 in the 50S subunit, bridge B1a, have a similar effect (40).

In the fully rotated ribosome, RRF binds in the P-site and A-site cleft of the 50S subunit, precluding tRNA binding in either site. Its three-helix bundle domain (domain I) runs nearly parallel to the subunit interface, with alpha helix 3 packed tightly against helix H71 in 23S rRNA (Fig. 4A). Mutations in this region result in lethal or temperature-sensitive phenotypes (41). In addition, conserved amino acids within the tip of RRF domain I (42) interact with rRNA nucleotides of the universally conserved P loop element of the peptidyl transferase center (Fig. 4A). These sets of interactions appear to be the same in both the unrotated and fully rotated states of the ribosome (33, 43), suggesting that they are necessary but not sufficient for the recycling mechanism.

Additional points of contact between RRF and the fully rotated ribosome occur between

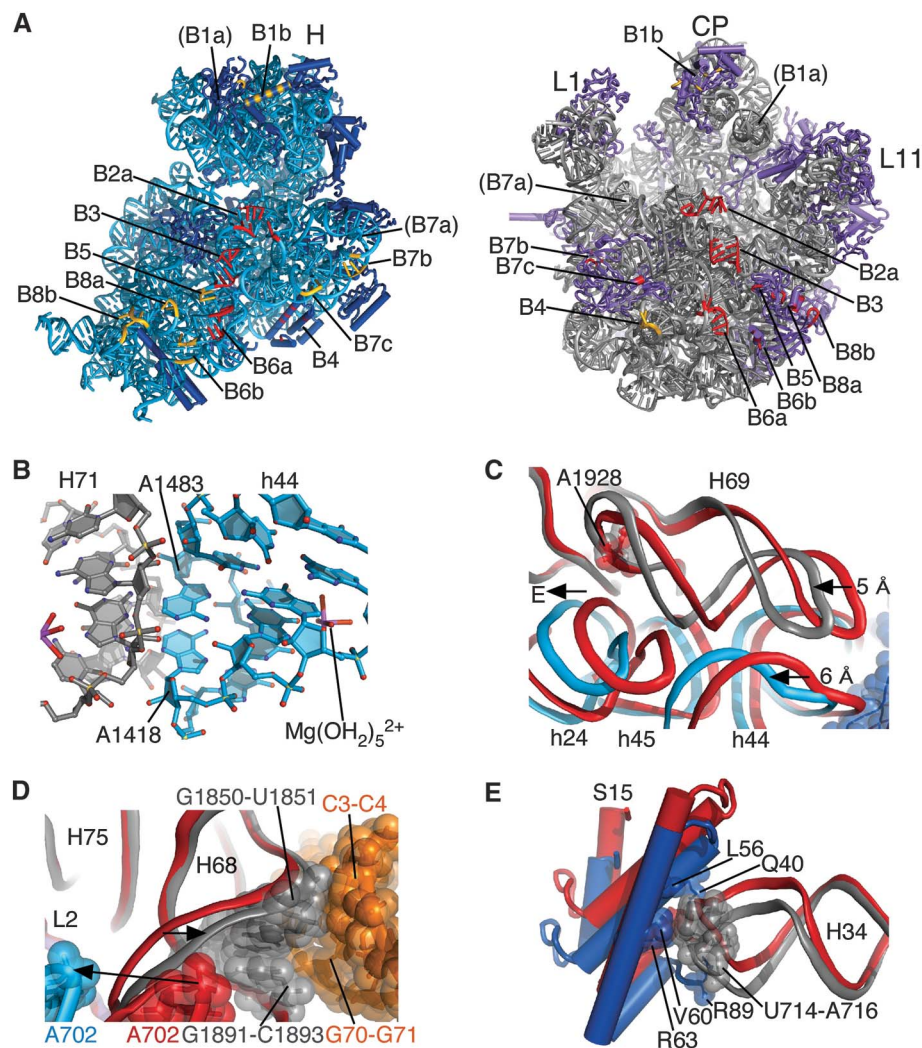


Fig. 3. Inter-subunit contacts in the fully rotated state. **(A)** Global view of inter-subunit contacts of the fully rotated state. Elements in each ribosomal subunit that contact rRNA in opposite subunit are color-coded red, whereas elements in each subunit that contact ribosomal proteins in the opposite subunit are color-coded gold. rRNAs and proteins are colored as in Fig. 1. Bridge numbering is adapted from (11, 26). The tip of helix H38 in bridge B1a is disordered in the present structures. The 30S subunit head region (H) and 50S subunit central protuberance (CP), L1 and L11 arms are labeled for reference. **(B)** Bridge B3 serves as the pivot of inter-subunit rotation. The Mg²⁺ ion involved in inner-sphere coordination to the tandem sheared GA pairs in 16S rRNA and a fully hydrated Mg²⁺ ion in 23S rRNA are also shown. rRNAs are colored as in Fig. 1. **(C)** Compression of helix H69 in 23S rRNA because of inter-subunit rotation. The direction of view is similar to Fig. 1. Color coding of the fully rotated ribosome (R) is as in Fig. 1, with unrotated ribosome (U) in red. Nucleotide A1928 in 23S rRNA, nearly invariant in position, is shown for reference. Helices in 16S rRNA are labeled “h” and in 23S rRNA are labeled “H.” **(D)** Movement of H68 because of disruption of A702 interactions and packing with P/E tRNA. Nucleotides involved in H68 packing with P/E tRNA are indicated. Elements of the fully rotated ribosome are colored as in Fig. 1. Elements of the unrotated ribosome are shown in red. Arrows indicate movement from the unrotated to fully rotated state. **(E)** Bridge B4 in the fully rotated state compared with that in the unrotated state (R₀, red). Residues involved in direct contact in the fully rotated state are shown. Coloring for the fully rotated state is as in Fig. 1.

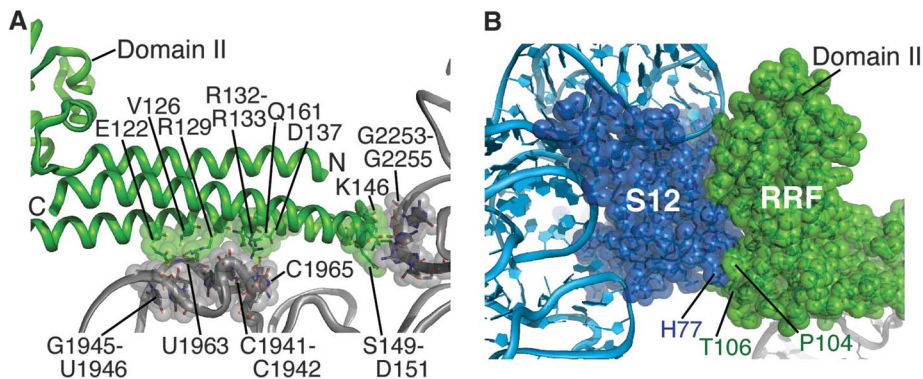


Fig. 4. RRF interactions with the ribosome in the fully rotated state. **(A)** Contacts between RRF domain I and the P and A sites of the 50S subunit. Amino acids in RRF (green) and nucleotides in 23S rRNA (gray) in direct contact are shown. Helix H69 and the 30S subunit are behind the view shown. **(B)** Contacts between RRF and protein S12 in the 30S subunit. Amino acids at the junction of RRF domains I and II that interact closely with S12 are indicated. RRF, S12, and rRNAs are colored as in Fig. 1.

conserved amino acids near the junction of domains I and II in RRF and ribosomal protein S12 of the small subunit (Fig. 4B) (42). Domain II of RRF is more constrained in its position in the ratcheted state as compared with its location in the unratcheted ribosome (33, 43). As suggested by cryo-EM reconstructions of the ribosome in complexes with RRF (14, 15), RRF domain II probably serves a steric function in ribosome recycling. Docking of EF-G from a cryo-EM reconstruction of the ribosome in a rotated conformation related to translocation (10) onto the ratcheted 70S ribosome structure determined here shows substantial overlap between domain II of RRF and domains IV and V of EF-G (fig. S6). Thus, EF-G binding to the RRF-bound ribosome probably entails large-scale rearrangements in RRF, EF-G, and the ribosome (15).

When compared with other structures, the structure of the fully rotated state of the ribosome provides critical insights into the molecular description of the ratcheting mechanism in translation. Because simple mRNAs can be translated in the absence of exogenous factors like EF-G (44), the ribosome itself serves as a Brownian ratchet (2, 45), with tRNA substrates probably serving as the “teeth.” A notable feature of the ratcheting mechanism is the use of RNA secondary structural elements to control large-scale conformational rearrangements in the ribosome. These include RNA stem-loops in bridges B2a and B4 that adjust as the 30S subunit rotates relative to the 50S subunit (8, 11, 15, 46, 47); helix H68 in 23S rRNA adjacent to bridge B7a and P/E tRNA; RNA helices H76 and H42 in the L1 and L11 arms of the large subunit, respectively (1, 2, 11, 37, 48); and helix h28 in 16S rRNA which directs swiveling of the 30S subunit head domain (25). Helix h28 probably serves as the “spring” in the ratcheting process, helping to position the “pawl” between the small subunit P and E sites (3, 10, 25, 45). The hinge-like motion in P/E tRNA observed here, when compared with P/P tRNA, suggests that the conserved tertiary structure of tRNA is required not only for mRNA

decoding (20, 21, 49) but also for translocation, termination, and ribosome recycling (10, 50). Intact P-site tRNA is required for translocation (51), a requirement that may in part be due to a need for a large distortion of tRNA in the P/E binding site. This distortion may be used to tune the energetics of the transition between the pretranslocation state and posttranslocation state of the ribosome. Future structural studies of ribosome complexes with EF-G will be required to explain how this factor controls the conformational events described here to accelerate translocation and ribosome recycling.

References and Notes

1. T. M. Schmeing, V. Ramakrishnan, *Nature* **461**, 1234 (2009).
2. J. B. Munro, K. Y. Sanbonmatsu, C. M. Spahn, S. C. Blanchard, *Trends Biochem. Sci.* **34**, 390 (2009).
3. J. A. Dunkle, J. H. Cate, *Annu. Rev. Biophys.* **39**, 227 (2010).
4. J. Frank, R. K. Agrawal, *Nature* **406**, 318 (2000).
5. D. Moazed, H. F. Noller, *Nature* **342**, 142 (1989).
6. Y. P. Semenkova, M. V. Rodnina, W. Wintermeyer, *Nat. Struct. Biol.* **7**, 1027 (2000).
7. A. V. Zavialov, M. Ehrenberg, *Cell* **114**, 113 (2003).
8. W. Zhang, J. A. Dunkle, J. H. Cate, *Science* **325**, 1014 (2009).
9. N. Fischer, A. L. Konevega, W. Wintermeyer, M. V. Rodnina, H. Stark, *Nature* **466**, 329 (2010).
10. A. H. Ratje *et al.*, *Nature* **468**, 713 (2010).
11. A. Ben-Shem, L. Jenner, G. Yusupova, M. Yusupov, *Science* **330**, 1203 (2010).
12. Materials and methods are available as supporting material on Science Online.
13. L. Lancaster, M. C. Kiel, A. Kaji, H. F. Noller, *Cell* **111**, 129 (2002).
14. R. K. Agrawal *et al.*, *Proc. Natl. Acad. Sci. U.S.A.* **101**, 8900 (2004).
15. N. Gao *et al.*, *Mol. Cell* **18**, 663 (2005).
16. S. H. Sternberg, J. Fei, N. Prywes, K. A. McGrath, R. L. Gonzalez Jr., *Nat. Struct. Mol. Biol.* **16**, 861 (2009).
17. A. Savelsbergh, M. V. Rodnina, W. Wintermeyer, *RNA* **15**, 772 (2009).
18. F. Brandt *et al.*, *Cell* **136**, 261 (2009).
19. M. Selmer *et al.*, *Science* **313**, 1935 (2006).
20. T. M. Schmeing *et al.*, *Science* **326**, 688 (2009).
21. R. M. Voorhees, T. M. Schmeing, A. C. Kelley, V. Ramakrishnan, *Science* **330**, 835 (2010).
22. Single-letter abbreviations for the amino acid residues are as follows: A, Ala; C, Cys; D, Asp; E, Glu; F, Phe; G, Gly; H, His; I, Ile; K, Lys; L, Leu; M, Met; N, Asn; P, Pro; Q, Gln; R, Arg; S, Ser; T, Thr; V, Val; W, Trp; and Y, Tyr. Single-letter abbreviations for nucleotide

residues are as follows: A, adenosine; C, cytidine; G, guanosine; and U, uridine.

23. R. Lill, J. M. Robertson, W. Wintermeyer, *EMBO J.* **8**, 3933 (1989).
24. T. M. Schmeing, P. B. Moore, T. A. Steitz, *RNA* **9**, 1345 (2003).
25. K. Bokov, S. V. Steinberg, *Nature* **457**, 977 (2009).
26. B. S. Schuwirth *et al.*, *Science* **310**, 827 (2005).
27. J. H. Cate *et al.*, *Science* **273**, 1678 (1996).
28. C. L. Shenvi, K. C. Dong, E. M. Friedman, J. A. Hanson, J. H. Cate, *RNA* **11**, 1898 (2005).
29. J. J. Cannone *et al.*, *BMC Bioinformatics* **3**, 2 (2002).
30. D. N. Ermolenko *et al.*, *Nat. Struct. Mol. Biol.* **14**, 493 (2007).
31. P. V. Cornish, D. N. Ermolenko, H. F. Noller, T. Ha, *Mol. Cell* **30**, 578 (2008).
32. R. E. Stanley, G. Blaha, R. L. Grodzicki, M. D. Strickler, T. A. Steitz, *Nat. Struct. Mol. Biol.* **17**, 289 (2010).
33. M. A. Borovinskaya *et al.*, *Nat. Struct. Mol. Biol.* **14**, 727 (2007).
34. M. B. Feldman, D. S. Terry, R. B. Altman, S. C. Blanchard, *Nat. Chem. Biol.* **6**, 54 (2010).
35. J. H. Cate *et al.*, *Science* **273**, 1696 (1996).
36. J. S. Feinberg, S. Joseph, *Proc. Natl. Acad. Sci. U.S.A.* **98**, 11120 (2001).
37. M. Valle *et al.*, *Cell* **114**, 123 (2003).
38. J. Frank, H. Gao, J. Sengupta, N. Gao, D. J. Taylor, *Proc. Natl. Acad. Sci. U.S.A.* **104**, 19671 (2007).
39. A. R. Cukras, R. Green, *J. Mol. Biol.* **349**, 47 (2005).
40. T. Komoda *et al.*, *J. Biol. Chem.* **281**, 32303 (2006).
41. L. Janosi *et al.*, *J. Mol. Biol.* **295**, 815 (2000).
42. H. Ashkenazy, E. Erez, E. Martz, T. Pupko, N. Ben-Tal, *Nucleic Acids Res.* **38** (Web Server issue), W529 (2010).
43. A. Weixlbaumer *et al.*, *Nat. Struct. Mol. Biol.* **14**, 733 (2007).
44. L. P. Gavrilova, O. E. Kostiashekina, V. E. Koteliashnik, N. M. Rutkevitch, A. S. Spirin, *J. Mol. Biol.* **101**, 537 (1976).
45. A. S. Spirin, *J. Biol. Chem.* **284**, 21103 (2009).
46. S. R. Connell *et al.*, *Mol. Cell* **25**, 751 (2007).
47. C. M. Spahn *et al.*, *EMBO J.* **23**, 1008 (2004).
48. M. Valle *et al.*, *Nat. Struct. Mol. Biol.* **10**, 899 (2003).
49. M. Valle *et al.*, *EMBO J.* **21**, 3557 (2002).
50. W. Li, J. Frank, *Proc. Natl. Acad. Sci. U.S.A.* **104**, 16540 (2007).
51. S. Joseph, H. F. Noller, *EMBO J.* **17**, 3478 (1998).
52. We thank K. Hamadani for purified RRF; K. Nierhaus for tRNA^{fMet} overexpression plasmids; K. Frankel, S. Classen, and G. Meigs for help with data measurement at the SIBYLS and 8.3.1 beamlines at the Advanced Light Source (ALS); R. Kanagalaghatta, D. Neau, F. Murphy, and I. Kourinov for help with data measurement at ID-24 at the Advanced Photon Source (APS); J. Headd for help with Phenix refinement; and J. Holton for useful crystallographic discussions. We also thank J. Doudna and H. Noller for helpful comments on the manuscript. Atomic coordinates and structure factors are deposited in the Protein Data Bank (accession codes 3R8N and 3R85 for the fully rotated state R_f, 3R80 and 3R8T for the unratcheted state R₀). This work was funded by the National Institutes of Health (GM65050 to J.H.D.C., GM079238 to S.C.B., and GM074127-04S1, GM088674, and P01-GM3210 project IV to J.S.R.), National Cancer Institute grant CA92584 for the SIBYLS and 8.3.1 beam lines at the ALS, and National Center for Research Resources grant RR-15301 for the Northeastern Collaborative Access Team beam lines at 24-ID at APS, and by the U.S. Department of Energy (DE-AC03 76SF00098 for the SIBYLS and 8.3.1 beamlines at the ALS, and DE-AC02-06CH11357 for the APS). M.B.F. is a trainee in the Weill Cornell/Rockefeller University/Sloan-Kettering Tri-Institutional MD-PhD Program supported by NIH Medical Scientist Training Program grant GM07739. J.N. is supported by a Human Frontiers in Science Program Postdoctoral Fellowship.

Supporting Online Material

www.sciencemag.org/cgi/content/full/332/6032/981/DC1

Materials and Methods

Figs. S1 to S6

Tables S1 to S3

References

Movies S1 and S2

10 January 2011; accepted 6 April 2011

10.1126/science.1202692